



ORIGINAL RESEARCH ARTICLE

Dissolution Behavior of Carbide in 4Cr13 Martensitic Stainless Steel during Austenitizing

Tianchi Ma, Bin Fu , Wei Guan, Yanhui Guo, Liming Fu, and Aidang Shan

Submitted: 29 August 2023 / Revised: 23 March 2024 / Accepted: 30 March 2024

The dissolution behavior of $M_{23}C_6$ carbide in 4Cr13 martensitic stainless steel during austenitizing and its effect on the microstructure and mechanical properties of this steel are investigated in this study. The samples of steel are heated at different austenitizing temperatures from 1000 to 1150 °C for 10–60 min. The results reveal that as the austenitizing temperature and time increase, the average initial austenite grain size increases, the carbide volume fraction decreases, and the average carbide size increases. The rapid dissolution of small carbides mainly contributes to the change in the average carbide size. The carbides can be completely dissolved in the matrix at 1150 °C for 30 min. After quenching, the hardness first increases and then decreases with increasing carbide dissolution degree. An increase in the hardness is related to an increase in the carbon content of the quenched martensite, and a decrease in the hardness is associated with an increase in the volume fraction of the retained austenite. Furthermore, a mathematical model is established to predict the volume fraction of carbides, which is in agreement with the experimental results.

Keywords austenitizing, carbide, dissolution behavior, model, martensite stainless steel

1. Introduction

4Cr13 martensitic stainless steel (hereinafter referred to as 4Cr13) is frequently used in surgical instruments, razor blades, bearings, and plastic molds due to its high hardness, wear resistance, and corrosion resistance (Ref 1–4). The microstructure of 4Cr13 consists of martensite and carbides, and a precipitate phase of carbides in stainless steel significantly influences the mechanical properties and corrosion performance of the steel (Ref 5–8).

The size and content of carbides in stainless steel significantly influence its properties. In high-wear applications such as cutting tools and turbine blades, some carbides need to exist in the martensite matrix to enhance wear resistance (Ref 9). In 440C high-carbon martensitic stainless steel, high-fraction and small carbides at an austenizing temperature of 950 °C provide a better strength-ductility balance of the sample than those at 1160 °C (Ref 10). Fine carbides can improve hardness and toughness by affecting the volume fraction of retained austenite (Ref 11). In contrast, coarse carbides eventually deteriorate the mechanical properties and corrosion resistance of stainless steel (Ref 12, 13). The complete dissolution condition in AISI 420 martensitic stainless steel is 1175 °C/15 min, and as the carbide volume fraction decreases, the retained austenite content increases and the initial austenite grains

coarsen (Ref 14). In 0.38C–13.6Cr martensitic stainless steel, carbides completely dissolve in the matrix at 1130 °C/45 min, and as the carbide content decreases, the distribution of Cr in the matrix becomes increasingly uniform, and the corrosion resistance of the steel increases (Ref 15, 16). According to different heating rate tests, carbides in 0.45C–13Cr martensitic stainless steel are fully dissolved within 60 s at temperatures between 1080 °C and 1175 °C (Ref 17). Therefore, it is necessary to consider the carbide dissolution behavior during solution treatment. Generally, commercial 4Cr13 is in an annealing state, the microstructure of which mainly consists of ferrite and many carbides. To obtain a good combination of mechanical properties and corrosion performance, commercial 4Cr13 usually needs to undergo solution treatment and quenching to obtain martensite, carbide, and retained austenite.

Heating temperature and holding time are known to have a significant influence on the volume fraction and size of carbides in quenched stainless steel (Ref 14, 16). However, most previous studies (Ref 14–17) on the solution treatment of 4Cr13 were focused on specific conditions and lacked coherent quantitative analysis of the carbide dissolution behavior. Furthermore, to the best of our knowledge, the changes in carbide size have not been studied in detail. To optimize the solution treatment of 4Cr13 and control the volume fraction of carbides, the changes in carbides during the solution treatment of 4Cr13 and the influences of the microstructural changes on the hardness were studied in this paper. Finally, a mathematical model was established to predict the volume fraction of carbides in 4Cr13 under different austenitizing conditions. This study could provide a reference for the solution treatment design of 4Cr13 in industry.

2. Materials and Methods

2.1 Materials and Processing

The as-received materials were commercial hot-rolled and annealed 4Cr13 with a thickness of 22 mm. The chemical composition of this material is shown in Table 1. Due to the

Tianchi Ma, Bin Fu, Wei Guan, and Yanhui Guo, School of Materials Science and Engineering, Shanghai Institute of Technology, 100 Haiquan Road, Shanghai 201418, People's Republic of China; Liming Fu and Aidang Shan, School of Materials Science and Engineering, Shanghai Jiao Tong University, 800 Dongchuan Road, Shanghai 200240, People's Republic of China. Contact e-mails: fubin@sit.edu.cn and lmfu@sjtu.edu.cn.

possible segregation in 4Cr13 steel plates, the core area of steel plates with good homogenization during austenitizing was selected as the research area (Ref 16). Figure 1 shows the phase equilibrium diagram of 4Cr13 martensitic stainless steel. According to this diagram, the carbide content changed significantly in the range of 1000–1150 °C, and some temperatures above 1000 °C were chosen to study the dissolution behavior of carbides. The samples were heated at four different austenitizing temperatures (1000 °C, 1050 °C, 1100 °C, and 1150 °C) and held at each temperature for three different times (10 min, 30 min, and 60 min) before oil quenching.

2.2 Microscopy

The samples used for the experiment were subjected to electrochemical polishing after mechanical polishing to remove the surface strain layer. The electrolyte was a perchloric acid solution (5 ml of HClO₄ + 95 ml of C₂H₅OH). Then, the samples were etched in a saturated HCl-FeCl₃ solution. The phase compositions of the samples were analyzed with a Shimadzu XRD-6000 diffractometer. The Cu target K α radiation source was used as the light source in the experiment. The scanning speed was 2°/min, the scanning voltage and the scanning current were 35 kV and 200 mA, respectively, and the diffraction angle range of 2 θ was 40° ~ 100°. The microstructure was observed by an optical microscope (Leica MEF4A) and a JSM-7800F superresolution field emission scanning electron microscope (SEM). An energy dispersive spectrometer (EDS) equipped with an SEM was used to examine the elemental composition. Medibang Paint software was used to process the micrographs obtained by the SEM. For each condition, five photos were selected, and the regions represented by carbide particles were filled with other colors with high contrast. Then, Image-Pro Plus software was used to measure the content and size of the undissolved carbide.

2.3 Mechanical Properties

A 402SXV Vickers microhardness tester was used to test the hardness of the samples. The microhardness tester probe was a pyramidal diamond probe, the load was set to 500 g, and the loading time was 20 s. At least 10 experimental data points were detected for each sample, and the average value was calculated as the hardness.

3. Results and Discussion

3.1 X-ray Diffraction Pattern Analysis

Figure 2(a) shows the XRD patterns of the different samples. The α (110), α (200), and α (211) peaks, which represent the BCC structure, appear in all the samples. The BCC peak in the initial samples represents ferrite, and that in

Table 1 Chemical composition of the experimental steel (wt.%)

C	Cr	Mn	Ni	Si	Co	V	Fe
0.4	12.02	0.62	0.5	0.71	0.26	0.24	Bal.

the quenched sample represents martensite (the hardness of the initial sample is 233 HV0.5, while the hardness of the quenched sample is above 560 HV0.5). The γ phase appears at temperatures above 1050 °C. The carbon content in austenite significantly increases with increasing temperature, which improves the stability of austenite; thus, austenite cannot transform to martensite completely during quenching.

Figure 2(b) shows a locally magnified view of Fig. 2(a) in the range of 46–53°. The peaks representing M₂₃C₆ carbide appear in the initial sample and in samples heated at 1000 °C for 30 min. The peaks are attributed to the (440), (531), and (600) planes of M₂₃C₆ from left to right (Ref 16). When the austenitizing temperature exceeds 1050 °C, the peak of M₂₃C₆ disappears, indicating that the carbide content decreases to a very low level.

3.2 Microstructure

Figure 3(a) shows the microstructure of the sample after austenitizing at 1000 °C for 30 min, which consists of white spherical particles and a black–gray matrix. Figure 3(b) shows the elemental distribution obtained via line-scanning analysis with an EDS. According to the characteristics of M₂₃C₆, the Fe-poor and Cr-rich regions (the region with white spherical particles) correspond to the location of the M₂₃C₆ carbide particles, and the black–gray region corresponds to the martensite matrix. In Fig. 3(a), some microregions (marked as A, B, C, D, E, and F) are selected for further compositional analysis. The analysis results are shown in Table 2. The Fe and Cr content ratios in A, B, C, and D suggest that the type of carbide in the microstructure is M₂₃C₆ (Ref 18). The content of Cr in the M₂₃C₆ carbide (33–54%) is significantly greater than that in the matrix (approximately 13%). Furthermore, the Cr content in the carbide center increases with increasing carbide size. In addition, the content of Si in the matrix is significantly greater than that in M₂₃C₆, which indicates that Si is not a carbide-forming element.

Figure 4 shows the microstructures of the initial sample and the samples after quenching at different austenitizing temperatures for 30 min. Figure 5 shows the microstructures of the samples after quenching at 1050 °C for different durations. The

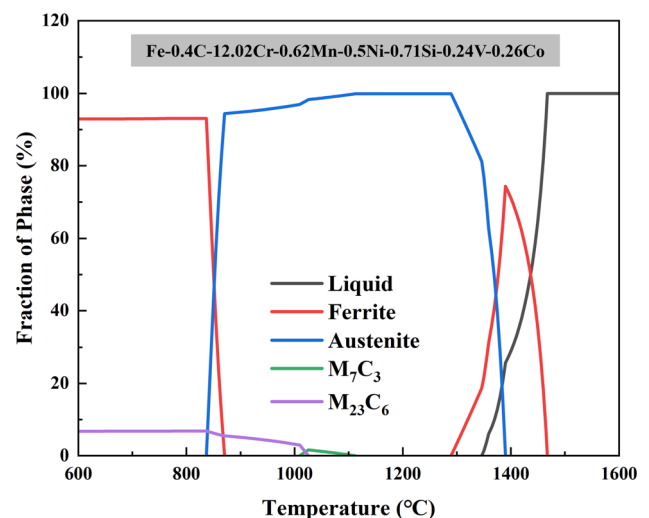


Fig. 1 Phase equilibrium diagram of 4Cr13 martensitic stainless steel

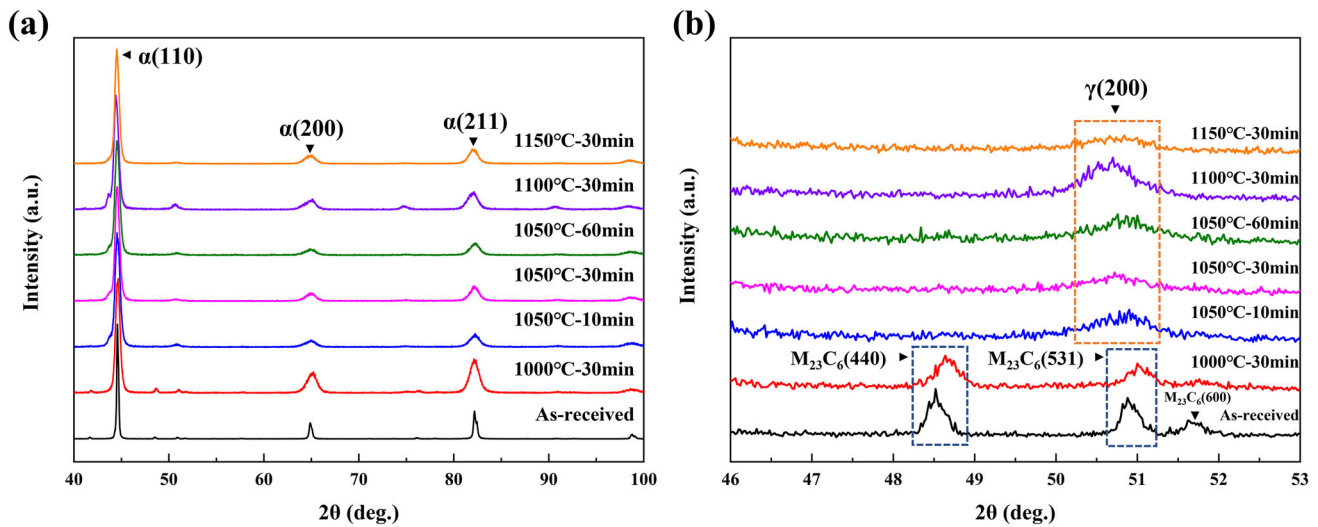


Fig. 2 (a) XRD patterns of samples after solution treatment under different austenitizing conditions (b) Locally magnified view of (a) in the range of 46-53°

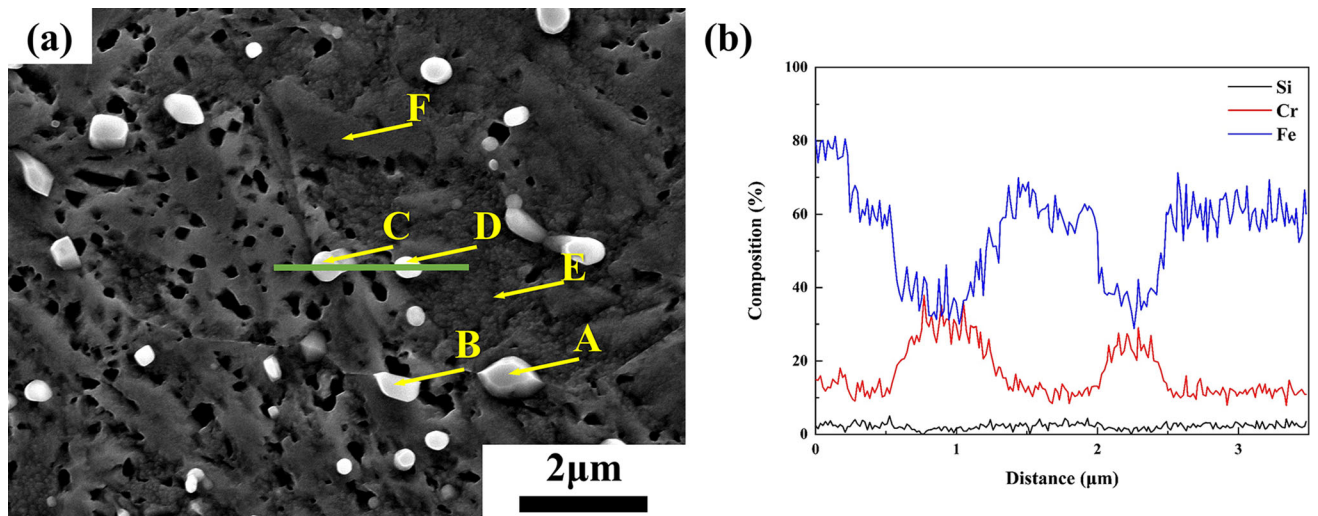


Fig. 3 (a) SEM image of the 1000 °C/30 min sample and (b) EDS image along the line shown in (a) across the carbides

Table 2 EDS component analysis of the sample (corresponding to selected points in Fig. 2(a))

Points	Chemical composition, in wt.%				
	Fe	Cr	Mn	Si	V
A	37.07	54.25		0.36	1.39
B	50.93	39.72		0.90	1.13
C	48.91	39.93	0.50	0.92	1.25
D	55.57	33.54	0.33	1.20	1.13
E (Matrix)	79.97	12.34	0.79	1.79	0.44
F (Matrix)	80.58	13.20	0.99	1.76	

initial sample is composed of ferrite and carbides. A martensite matrix and undissolved carbides can be observed in the samples after quenching. The carbides in the initial sample are mostly round and rectangular, most of the carbides are less than 1 μm in size, and the edges of the carbides are relatively smooth. In contrast, the carbides in the quenched sample gradually became round as the carbide volume fraction decreases. With increasing

austenitizing temperature and holding time, the volume fraction of carbides decreases gradually. When the temperature reaches 1150 °C, the carbides completely dissolve in the matrix. However, the average carbide size increases gradually with increasing solubility. The number of small particles decreases, while the number of large particles increases, as shown in Fig. 4(f) and 5(f). In particular, the undissolved carbide particles are almost all large (0.5 ~ 1 μm) at 1100 °C and finally dissolve in the matrix at 1150 °C.

This phenomenon may be related to small particles being more soluble than large particles. The total interfacial energy of small carbides is high, and a short diffusion distance is required for Cr (Ref 19-21). When carbides are dissolved, Cr diffuses into the matrix; thus, the ratio of Cr/Fe in carbides can be used as the basis for determining the degree of dissolution of carbides (Ref 22). According to the contents of Cr and Fe in the carbides of different sizes under the same conditions in Table 2, the content of Cr in the small carbides is lower than that in the large carbides.

Figure 6 shows the OM images of the quenched samples after austenitizing at different temperatures. The microstructure

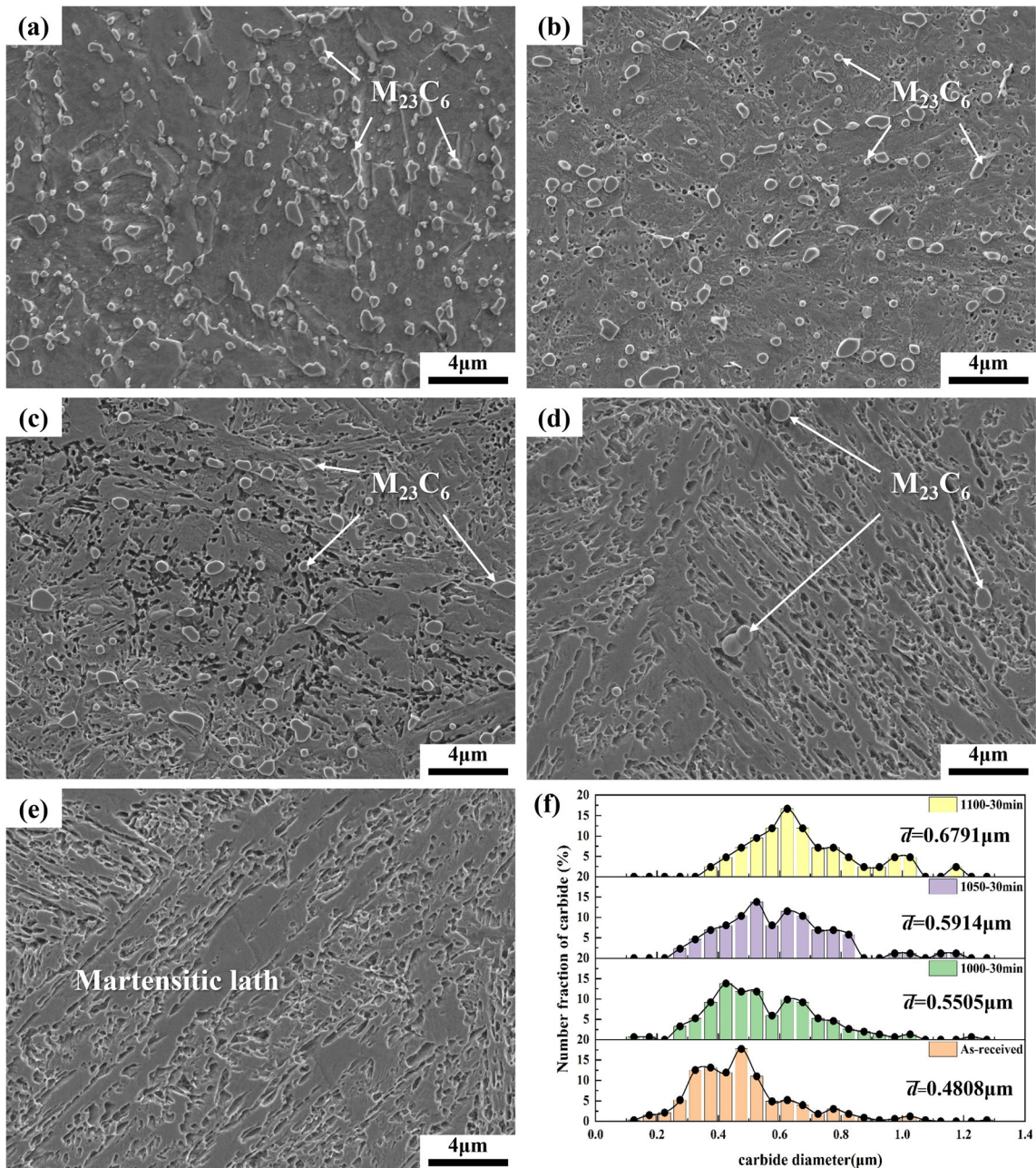


Fig. 4 SEM images of the (a) as-received sample, (b) 1000 °C/30 min sample, (c) 1050 °C/30 min sample, (d) 1100 °C/30 min sample, (e) 1150 °C/30 min sample. (f) Statistical diagram of the carbide size in the samples held at different austenizing temperatures for 30 min

of quenched 4Cr13 includes a martensite matrix and different amounts of carbides. The average grain size of the prior austenite is directly measured with the initial austenite grain boundaries. The average grain sizes of the initial austenite in the samples heated at 1000 °C, 1050 °C, 1100 °C and 1150 °C for 30 min are approximately 10 μm, 60 μm, 100 μm, and 200 μm, respectively. The prior austenite grain size increases with increasing temperature. In addition, the carbide content decreases at relatively high temperatures, which leads to a weakening of the carbide pinning effect, and the initial austenite grains further coarsen.

3.3 Hardness

Figure 7 shows the hardness results of the samples under different austenizing temperatures and times. The hardnesses of the samples range from 562 to 650 HV0.5, and a peak hardness of 650 HV0.5 is observed at 1100 °C for 30 min. As the degree of carbide dissolution increases, the hardness first increases and then decreases. At the beginning of dissolution, the carbon in the carbides gradually dissolves into the matrix, resulting in an increase in hardness. With a further increase in the carbon content in the matrix during dissolution, the stability of austenite improves, and the amount of retained austenite

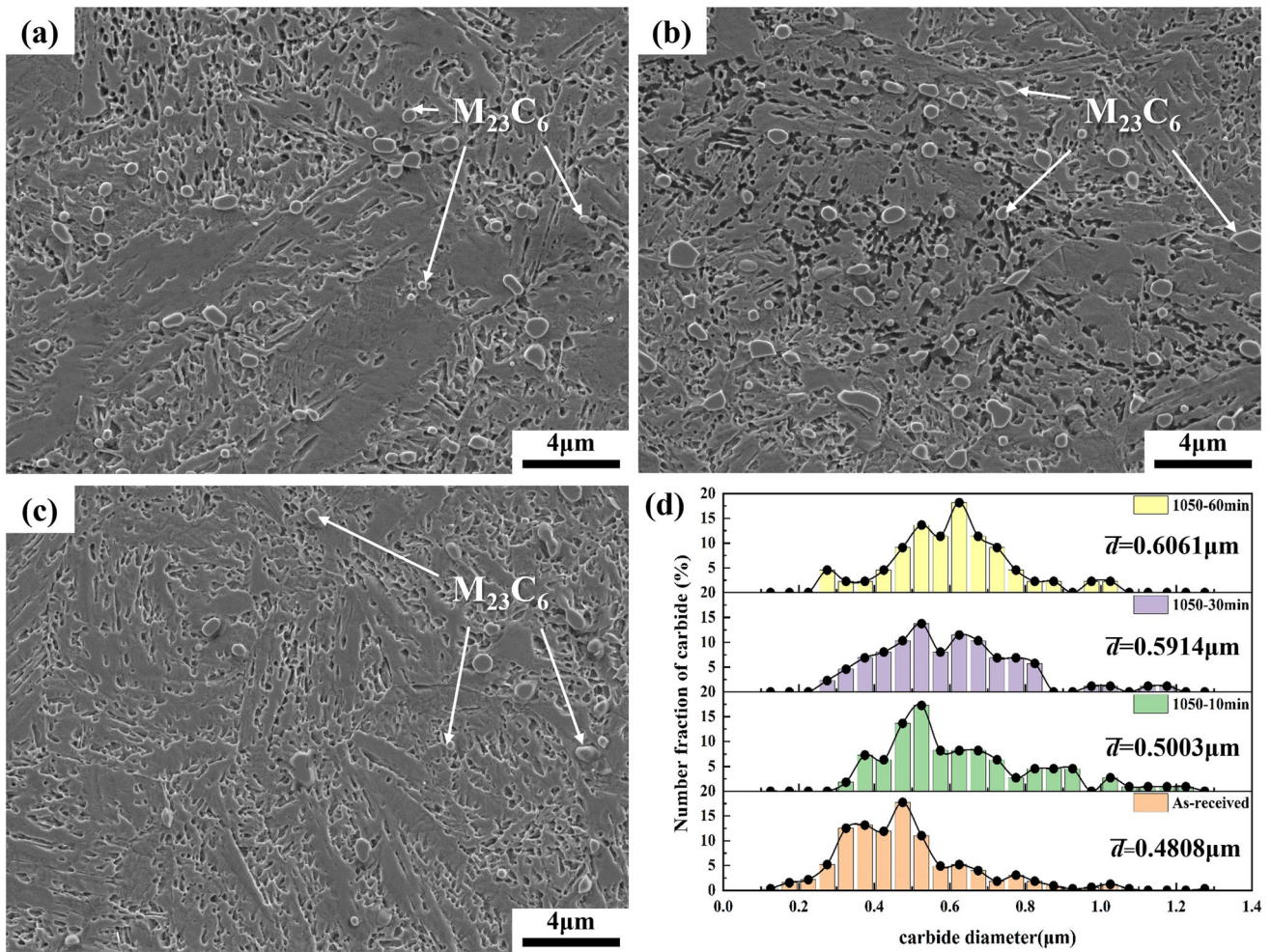


Fig. 5 SEM images of the (a) 1050 °C/10 min sample, (b) 1050 °C/30 min sample, (c) 1050 °C/60 min sample. (d) Statistical diagram of the carbide size in the samples held at 1050 °C for different austenitizing times

correspondingly increases after quenching. Simultaneously, the prior austenite grains are further coarsened due to the weakening of the carbide pinning effect. The above two sides decrease the hardness.

3.4 Carbide Dissolution Model

To quantitatively describe the changes in carbides in 4Cr13 with austenitizing temperature and time during the process, a model is designed to predict the volume fraction of carbides in the process of austenitizing.

According to the dissolution model of chromium carbide in an Fe-C-Cr system alloy proposed by Sozykina (Ref 23), the change in the volume fraction of carbides with austenitizing temperature and time can be given by the Avrami-type equation (Eq 1):

$$f_c = f_c^{eq} + (f_c^{in} - f_c^{eq}) \cdot \exp \left[- \left(\frac{(f_c^{in})^{4/3}}{(f_c^{in} - f_c^{eq}) \cdot (1 - f_c^{eq})} \cdot \beta_1 \exp \left(- \frac{Q}{RT} \right) \cdot t \right)^{1/2} \right] \quad (\text{Eq 1})$$

where f_c represents the volume fraction of carbides at temperature T after time t , f_c^{in} represents the volume fraction

of carbides at the initial state, f_c^{eq} represents the volume fraction of carbides at the equilibrium state, and Q represents the activation energy required for carbide dissolution, and its value is related to the composition of the carbide, namely, the atomic fraction y_{Cr} of Cr in the carbide lattice, which is given by Eq 2 (Ref 23):

$$Q = \begin{cases} 258.0 - 116.5y_{Cr} & (y_{Cr} \leq 0.5732) \\ 115.0 + 133.0y_{Cr} & (y_{Cr} > 0.5732) \end{cases} \quad (\text{kJmol}^{-1}) \quad (\text{Eq 2})$$

The former term of the index is dependent on the volume fraction of carbides, which is given by Eq 3 (Ref 23):

$$\ln \beta_1 = 17.406 - 9.653f_c^{eq} \quad (\text{min}^{-1}) \quad (\text{Eq 3})$$

According to Lee's thermodynamic study on the Fe-C-Cr ternary alloy system (Ref 24), we take $y_{Cr}=0.5$ as the atomic fraction of Cr in the carbide of 4Cr13 used in this study to obtain $Q = 200 \text{ kJmol}^{-1}$, where f_c^{in} is the content of carbide measured at the initial state of 4Cr13 in this study, while f_c^{eq} at different temperatures is obtained by thermodynamic calculation software (JMat Pro). Figure 8 shows the carbide mass fraction calculated at different austenitizing temperatures when the equilibrium state is reached. In practice, the initial carbide fraction in 4Cr13 is generally greater than the calculated initial carbide fraction in the equilibrium state (denoted as f_{c1}^{in}); thus,

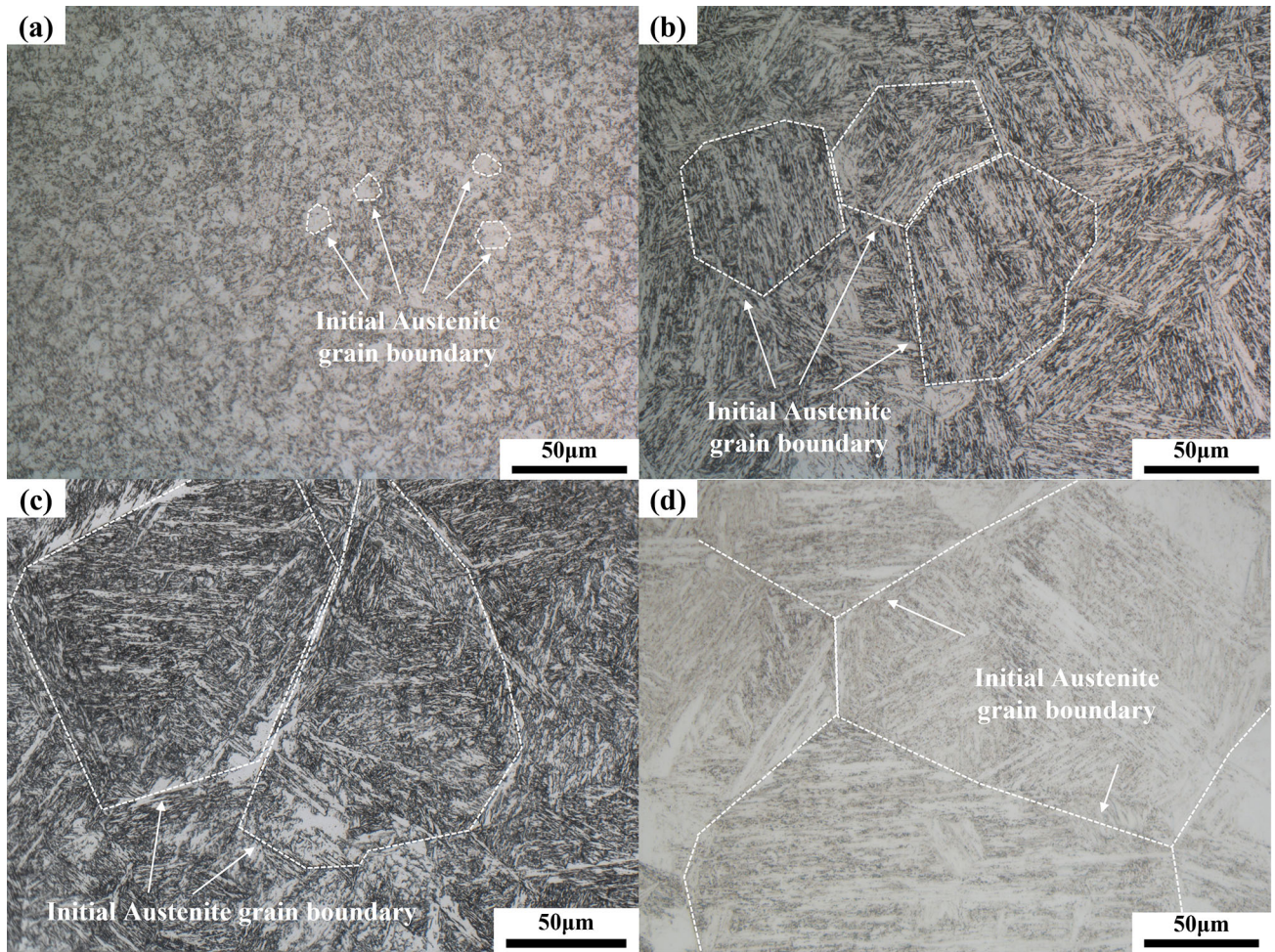


Fig. 6 Optical microscopy images at (a) 1000 °C/30 min sample, (b) 1050 °C/30 min sample, (c) 1100 °C/30 min sample, (d) 1150 °C/30 min sample

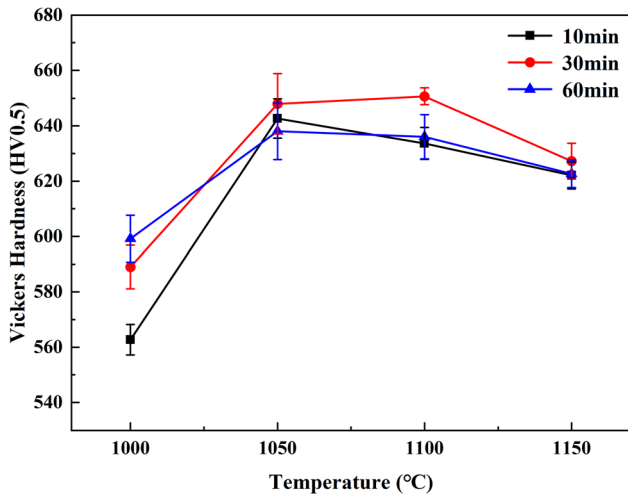


Fig. 7 Hardnesses of the samples after solution treatment under different austenitizing conditions

the f_c^{eq} value required by the model calculation at different austenitizing temperatures needs to be converted to the calculated value (denoted as f_{c1}^{eq}) in equal proportion, as shown in Eq 4:

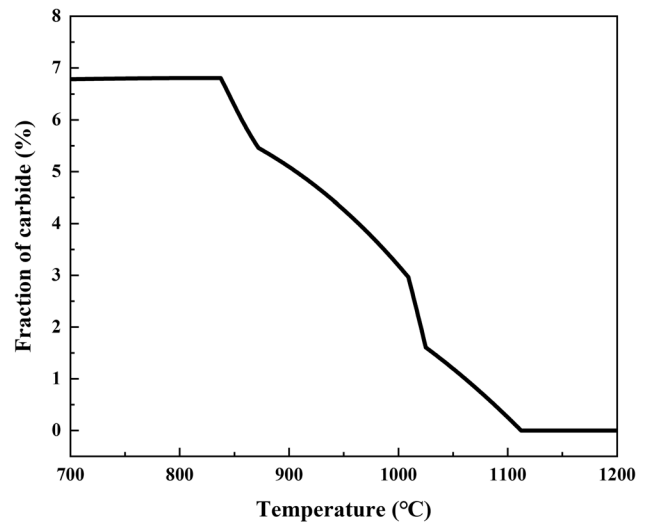


Fig. 8 Fraction of carbides in the equilibrium state at different austenitizing temperatures calculated by JMat Pro

$$\frac{f_{c1}^{in}}{f_{c1}^{eq}} = \frac{f_c^{in}}{f_c^{eq}} \quad (\text{Eq 4})$$

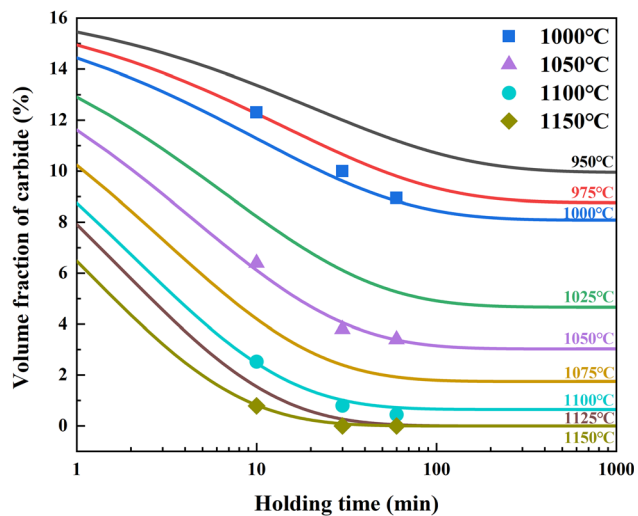


Fig. 9 The volume fraction of carbides in 4Cr13 after solution treatment under different austenitizing conditions: experimental data and model predictions

Substituting the above parameters into Eq 1, Figure 9 shows the calculated variations in the volume fraction of carbides in 4Cr13 under different austenitizing temperatures and times. The experimental data obtained in this study are represented by symbols of different shapes. The time needed to reach dissolution equilibrium gradually decreases with increasing temperature, from approximately 700 min at 950 °C to approximately 30 min at 1150 °C. The volume fraction of carbides in the equilibrium state decreases with increasing temperature, and carbides can be fully dissolved in the matrix at 1125 °C. The experimental data in this study agree with the predicted results of the model very well. Therefore, this model makes it easy and reliable to predict carbide dissolution behavior in 4Cr13 at different austenitizing temperatures and times.

4. Conclusions

The carbide dissolution behavior in 4Cr13 martensitic stainless steel was studied at austenitizing temperatures ranging from 1000 to 1150 °C and times ranging from 10 to 60 min. The main results were as follows:

1. With increasing austenitizing temperature and time, the average initial austenite grain size increases, and the carbide volume fraction decreases; however, the average size of the undissolved carbides increases. This phenomenon is related to the rapid dissolution of small carbides. $M_{23}C_6$ carbides are fully dissolved in steel and do not precipitate during quenching at 1150 °C for 30 min.
2. After quenching, the hardness of 4Cr13 first increases and then decreases with increasing carbide dissolution degree and reaches 650 HV0.5 at 1100 °C for 30 min. The increase in hardness is related to the increase in carbon content in the quenched martensite, and the decrease in hardness is associated with the increase in the volume fraction of the retained austenite.
3. A dissolution model of carbides in 4Cr13 is established. The experimental data agree well with the predicted re-

sults of the model, which can accurately predict the volume fraction of undissolved carbides in 4Cr13 easily during austenitization.

Conflict of interest

No potential conflict of interest was reported by the author(s).

References

1. I. Yadroitsev, P. Krakhmalev, and I. Yadroitsava, Hierarchical Design Principles of Selective Laser Melting for High-Quality Metallic Objects, *Addit. Manuf.*, 2015, **7**, p 45–56. <https://doi.org/10.1016/j.addma.2014.12.007>
2. N. Momenzadeh, S.D. Nath, T.A. Berfield, and S.V. Atre, In Situ Measurement of Thermal Strain Development in 420 Stainless Steel Additive Manufactured Metals, *Exp. Mech.*, 2019, **59**(6), p 819–827. <https://doi.org/10.1007/s11340-019-00513-3>
3. K. Saeidi, D.L. Zapata, F. Lofaj, L. Kvetkova, J. Olsen, Z. Shen, and F. Akhtar, Ultra-High Strength Martensitic 420 Stainless Steel with High Ductility, *Addit. Manuf.*, 2019, **29**, 100803. <https://doi.org/10.1016/j.addma.2019.100803>
4. A.N. Isfahany, H. Saghafian, and G. Borhani, The Effect of Heat Treatment on Mechanical properties and Corrosion Behavior of AISI420 Martensitic Stainless Steel, *J. Alloy. Compd.*, 2011, **509**(9), p 3931–3936. <https://doi.org/10.1016/j.jallcom.2010.12.174>
5. S.K. Bhambri, Intergranular Fracture in 13 wt.% Chromium Martensitic Stainless Steel, *J. Mater. Sci.*, 1986, **21**(5), p 1741–1746. <https://doi.org/10.1007/BF0114734>
6. M. Harwarth, A. Brauer, Q. Huang, M. Pourabdoli, and J. Mola, Influence of Carbon on the Microstructure Evolution and Hardness of Fe-13Cr-xC (x = 0-0.7 wt.%) Stainless Steel, *Materials*, 2021, **14**(17), p 5063. <https://doi.org/10.3390/ma14175063>
7. S.D. Nath, H. Irrinki, G. Gupta, M. Kearns, O. Gulsoy, and S. Atre, Microstructure-Property Relationships of 420 Stainless Steel Fabricated By Laser-Powder Bed Fusion, *Powder Technol.*, 2019, **343**, p 738–746. <https://doi.org/10.1016/j.powtec.2018.11.075>
8. H. Hill, U. Raab, S. Weber, W. Theisen, M. Wollmann, and L. Wagner, Influence of Heat Treatment on the Performance Characteristics of a Plastic Mold Steel, *Steel Res. Int.*, 2011, **82**(11), p 1290–1296. <https://doi.org/10.1002/srin.201100098>
9. J. Li, T. He, P. Zhang, L. Cheng, and L. Wang, Effect of Large-Size Carbides on the Anisotropy of Mechanical Properties in 11Cr-3Co-3W Martensitic Heat-Resistant Steel for Turbine High Temperature Blades in Ultra-Supercritical Power Plants, *Mater Charact.*, 2020, **159**, 110025. <https://doi.org/10.1016/j.matchar.2019.110025>
10. J. Syarif, M.H. Yousuf, Z. Sajuri, A.H. Baghdadi, M. Merabtene, and M.Z. Omar, Effect of Partial Solution Treatment Temperature on Microstructure and σ of 440C martensitic σ , *Metals.*, 2020, **10**(5), p 694. <https://doi.org/10.3390/met10050694>
11. Q.-T. Zhu, J. Li, C.-B. Shi, and W.-T. Yu, Effect of Quenching Process on the Microstructure and Hardness of High-Carbon Martensitic Stainless Steel, *J. Mater. Eng. Perform.*, 2015, **24**(11), p 4313–4321. <https://doi.org/10.1007/s11665-015-1723-7>
12. S.K. Bonagani, V. Bathula, and V. Kain, Influence of Tempering Treatment on Microstructure and Pitting Corrosion of 13 wt.% Cr Martensitic Stainless Steel, *Corros. Sci.*, 2018, **131**, p 340–354. <https://doi.org/10.1016/j.corsci.2017.12.012>
13. A. Dalmau, C. Richard, and A. Igual-Muñoz, Degradation Mechanisms in Stainless Steels: Wear, Corrosion and Tribocorrosion Appraisal, *Tribol. Int.*, 2018, **121**, p 167–179. <https://doi.org/10.1016/j.triboint.2018.01.036>
14. L.D. Barlow and M. Du Toit, Effect of Austenitizing Heat Treatment on the Microstructure and Hardness of Martensitic Stainless Steel AISI 420, *J. Mater. Eng. Perform.*, 2012, **21**(7), p 1327–1336. <https://doi.org/10.1007/s11665-011-0043-9>
15. S.-Y. Lu, K.-F. Yao, Y.-B. Chen, M.-H. Wang, and X.-Y. Ge, Influence of Heat Treatment on the Microstructure and Corrosion Resistance of 13 Wt Pct Cr-Type Martensitic Stainless Steel, *Metall. Mater. Trans. A.*, 2015, **46**(12), p 6090–6102. <https://doi.org/10.1007/s11661-015-3180-1>

16. S.-Y. Lu, K.-F. Yao, Y.-B. Chen, M.-H. Wang, Y. Shao, and X.-Y. Ge, Effects of Austenitizing Temperature on the Microstructure and Electrochemical Behavior of a Martensitic Stainless Steel, *J. Appl. Electrochem.*, 2015, **45**(4), p 375–383. <https://doi.org/10.1007/s10800-015-0796-1>
17. C.G. de Andrés, G. Caruana, and L. Alvarez, Control of M₂₃C₆ Carbides in 0.45C-13Cr Martensitic Stainless Steel by Means of Three Representative Heat Treatment Parameters, *Mater. Sci. Eng. A*, 1998, **241**(1–2), p 211–215. [https://doi.org/10.1016/S0921-5093\(97\)00491-7](https://doi.org/10.1016/S0921-5093(97)00491-7)
18. E. Saliba and M. Grech, The Effect of Heat Treatment Parameters on the Microstructure and Torque Response of a 13 wt.% Cr Steel, *J. Magn. Magn. Mater.*, 2022, **541**, 168543. <https://doi.org/10.1016/j.jmm.2021.168543>
19. J.-H. Kang and P.E.J. Rivera-Díaz-del-Castillo, Carbide Dissolution in Bearing Steels, *Comput. Mater. Sci.*, 2013, **67**, p 364–372. <https://doi.org/10.1016/j.commatsci.2012.09.022>
20. J. Bratberg, J. Ågren, and K. Frisk, Diffusion Simulations of MC and M₇C₃ Carbide Coarsening in bcc and fcc Matrix Utilising New Thermodynamic and Kinetic Description, *Mater. Sci. Technol.*, 2013, **24**(6), p 695–704. <https://doi.org/10.1179/174328407x240954>
21. S.B. Hosseini, R. Dahlgren, K. Rytberg, and U. Klement, Dissolution of Iron-Chromium Carbides During White Layer Formation Induced by Hard Turning of AISI 52100 Steel, *Procedia. CIRP*, 2014, **14**, p 107–112. <https://doi.org/10.1016/j.procir.2014.03.095>
22. W. Song, P.-P. Choi, G. Inden, U. Prah, D. Raabe, and W. Bleck, On the Spheroidized Carbide Dissolution and Elemental Partitioning in High Carbon Bearing Steel 100Cr6, *Metall. Mater. Trans. A*, 2013, **45**(2), p 595–606. <https://doi.org/10.1007/s11661-013-2048-5>
23. A.S. Sozykina, K.Y. Okishev, A.G. Grebenshchikova, and D.A. Mirzaev, Kinetic Description of (Cr, Fe)₇C₃ Carbide Dissolution in Austenite of High-Carbon Fe-Cr-C Ternary Alloys, *Mater. Sci. Forum*, 2016, **870**, p 409–415. <https://doi.org/10.4028/www.scientific.net/MSF.870.409>
24. B.-J. Lee, On the Stability of Cr Carbides, *Calphad*, 1992, **16**(2), p 121–149. [https://doi.org/10.1016/0364-5916\(92\)90002-F](https://doi.org/10.1016/0364-5916(92)90002-F)

Publisher's Note Springer Nature remains neutral with regard to jurisdictional claims in published maps and institutional affiliations.

Springer Nature or its licensor (e.g. a society or other partner) holds exclusive rights to this article under a publishing agreement with the author(s) or other rightsholder(s); author self-archiving of the accepted manuscript version of this article is solely governed by the terms of such publishing agreement and applicable law.